Propulsion and Power Research 2020;9(3):289–303

http://ppr.buaa.edu.cn/

Propulsion and Power Research

www.sciencedirect.com

ORIGINAL ARTICLE

Slip flow of micropolar fluid through a permeable wedge due to the effects of chemical reaction and heat source/sink with Hall and ion-slip currents: an analytic approach

Khilap Singh[a], **Alok Kumar Pandey**[b,*], **Manoj Kumar**[a]

[a]*Department of Mathematics, Statistics and Computer Science, G. B. Pant University of Agriculture and Technology, Pantnagar, 263145, Uttarakhand, India*
[b]*Department of Mathematics, Graphic Era Deemed to Be University, Dehradun, 248002, Uttarakhand, India*

Received 14 August 2019; accepted 29 April 2020
Available online 14 September 2020

KEYWORDS

Chemical reaction;
Differential transformation method (DTM);
Hall current and ion slip;
Heat source/sink;
Micropolar fluid;
Slip velocity

Abstract This study focuses on the combined impact of heat source/sink and chemical reaction on slip flow of micropolar fluid through a permeable wedge in the existence of Hall and ion-slip currents. The governing highly non-linear PDEs were altered into a set of non-linear coupled ODEs by using similarity transformations. Differential transformation method (DTM) has been implemented in transformed ODEs equations. The comparison with previous literatures was performed and the data of this study was found to be in accordance with each other. The analytical solutions for skin-friction coefficients (surface drag forces), Nusselt and Sherwood numbers are depicted through graphs and tables. The study of boundary layer flow over a wedge surface plays an imperative role in the field of aerodynamics, heat exchanger, ground water pollution and geothermal system etc.

*Corresponding author.
E-mail address: mr.alokpandey1@gmail.com (Alok Kumar Pandey).
Peer review under responsibility of Beihang University.

Production and Hosting by Elsevier on behalf of KeAi

https://doi.org/10.1016/j.jppr.2020.04.006

Nomenclature

C	fluid concentration
C_{fx}	local skin friction coefficient in x direction
C_{fz}	local skin friction coefficient in z direction
D	chemical molecular diffusivity
Ec	Eckert number
I	inertial parameter
H	heat source/sink parameter
K	material parameter
k_0	thermal conductivity (unit: W/(m·K))
N	component of micro-rotation (unit: rad/s)
m	Falkner-Skan parameter
Nu	local Nusselt number
Pr	Prandtl number
Q_0	heat source/sink constant
Re	Reynolds number
R_0	chemical reaction rate constant
T	temperature of the fluid (unit: K)
T_∞	temperature of fluid far from the wedge
U	uniform velocity of fluid (unit: m/s)
u, v, w	velocity along x, y and z directions (unit: m/s)
(x, y, z)	Cartesian coordinates (unit: m)

Greek letters

β	Hartree pressure gradient parameter
β_e	Hall effect parameter
β_i	ion slip parameter
γ_0	spin-gradient viscosity (unit: N·s)
γ	chemical reaction parameter
η	non-dimensional distance
κ	vortex viscosity
μ	dynamic viscosity (unit: Pa·s)
υ	kinematic viscosity (unit: m^2/s)
ρ	density of the fluid (unit: kg/m^3)
σ	electrical conductivity (unit: S/m)
ψ	stream function
Ω	wedge angle

Subscripts

∞	free stream condition

1. Introduction

Various researchers have implemented the use of micro-polar fluids in different branches of science and engineering (contaminated and clean engine lubricants, complex biological structures, thrust bearing technologies, cervical flows, radial diffusion paint rheology, colloids and polymeric suspensions) during the last few decades. Eringen [1] formulated the theory of micropolar fluids. This theory stated that the material parameters, an additional independent vector field, the microrotation and new constitutive equations should be handled at the same time, along with the Newtonian fluid flow equations. Couple stress sustenance is a fascinating characteristic of this fluid class. Few anisotropic fluids, liquid crystals, animal and human blood, lubrication, colloidal suspension, polymeric fluids, turbulent shear flows and fluids containing certain additives are few illustrations of micro-polar fluids. Further, Eringen [2] expanded this micropolar fluid theory and termed as "thermomicropolar fluids".

The heat transfer and boundary layer flow and over a wedge shaped bodies has practical functions in lots of branches of engineering and science for instance geothermal systems, crude oil extractions, storage of nuclear waste and thermal insulation. Elbashbeshy and Dimian [3] examined the heat transfer flow over wedge surface. Xenos et al. [4] studied turbulent flow performance over wedge surface. Similarly, the impact of mixed convection over a vertical wedge was illustrated by Singh et al. [5]. Ishak et al. [6] discussed thermal behaviour of micro-polar fluid through wedge. Recently, many author's [7−13] studied fluid flow and heat transfer over a surface of wedge for various physical phenomena. The influence of heat generation/absorption on different geometry using nanofluid was studied by Refs. [14,15].

The magnetohydrodynamic (MHD) micro-polar fluid flow and heat transfer along with Hall and ion-slip currents has imperative relevances in engineering and science like as refrigeration coils, transmission lines, MHD accelerators, heating elements, power generators and electric transformers. Salem and El-Aziz [16] have considered Hall and chemical reaction effects on MHD flow over a stretching vertical surface. The ion-slip and hall currents, chemical reaction effects of on heat and mass transfer flow of magneto-micropolar fluid through a porous medium is investigated numerically by Elgazery [17]. Srinivasacharya and Kaladhar [18] analyzed the well-developed electrically conducting flow of couple stress fluid within the vertical plates in the existence of Hall and ion-slip effects. Recently, authors like [19−22] have investigated the problem on various fluid flows over different surface with effects of Hall and ion-slip. Bakr [23] proposed the chemical reaction impacts on free convection MHD heat and mass transfer flow over oscillatory plate using of micropolar fluid. Rashad et al. [24] studied the impacts of chemical reaction when fluid flow through a continuously moving vertical surface. The magneto-hydrodynamic stagnation point flow from stretching surface due to chemical reaction was made by Mabood et al. [25]. Mabood et al. [26] considered influence of radiation as well as chemical reaction on MHD flow of nanofluids in porous medium with viscous dissipation. Misra and Adhikary [27] investigated the impacts of chemical reaction on MHD physiological fluid flow in oscillatory channel.

The study related to MHD slip flow has shown promising efficiency in plenty of practical applications including non-mechanical MHD micropumps. A partial slip can be used for both stationary and moving boundary when a particulate fluid is used e.g. emulsions, suspensions, foams and polymer solutions. The importance of slip velocity effects in

different types of flow were studied by many researchers such as [28–35]. Damseh et al. [36] studied effect of suction/injection through micropolar fluid flows from a consistent stretched sheet. Rahman et al. [37] analyzed the heat transfer flow through an inclined plate using micropolar fluid with suction/injection. Rosali et al. [38] examined the flow of micropolar fluid from stretching/shrinking sheet in the presence of suction. Zaidi and Mohyud-Din [39] investigated suction/injection effects on magneto-hydrodynamic wall jet flow with Soret and Dufour.

The major objective of this study is to obtain the analytic solutions applying a scheme called the differential transformation method (DTM) for the heat and mass transfer flow through a permeable wedge with Hall and ion-slip currents using micro-polar fluid. The flow is along with the heat source/sink, uniform magnetic field, chemical reaction and slip velocity. The impacts of several significant parameters on velocities, temperature and concentration as well as on skin-frictions, Nusselt and Sherwood numbers are investigated. To the best of our memory such a study is not examined in the scientific literature.

2. Mathematical formulation

The incompressible, electrically conducting, steady viscous flow of heat and mass transfer of a micropolar fluid over a non-conducting permeable wedge in the existence of Hall and ion-slip currents is considered in present work. The slip velocity and heat source/sink impacts are also incorporated in this work. Figure 1 represents the flow model and geometry of the problem. This flow can be considered as the flow past a triangular or wedge shaped wick inside the heat pipe or heat exchanger. The authors use rectangular Cartesian coordinates (x, y, z) in which x, y and z are the distances measured alongside the wedge surface respectively. A strong magnetic field $B(x)$ is executed through electrically conducting fluid in y-axis. Thus, Hall and ion-slip currents affect the flow. The Hall current produces force in z-direction, inducing cross flow in the same direction that's why the flow becomes 3D. Under these assumptions that the fluid is non-magnetic and thermoelectric effect the equations in vector form are:

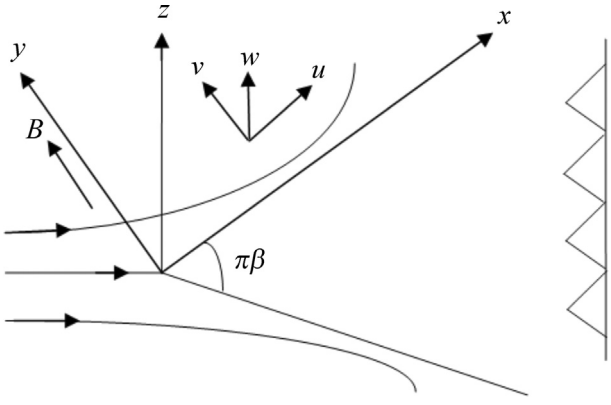

Figure 1 Physical model and coordinate system.

Conservation of mass:

$$div\vec{V} = 0 \tag{1}$$

Conservation of translational momentum:

$$\rho(\vec{V}\cdot\vec{\nabla})\vec{V} = -(\vec{\nabla}p) + (2\mu+\kappa)\vec{V}(\vec{\nabla}\cdot\vec{V}) - (\mu+\kappa)\vec{\nabla}\times(\vec{\nabla}\times\vec{V}) + \kappa(\vec{V}\times\vec{N}) + \vec{J}\times\vec{B} \tag{2}$$

Conservation of angular momentum (microrotation):

$$\rho(\vec{N}\cdot\vec{\nabla})\vec{N} = \gamma\vec{\nabla}(\vec{\nabla}\cdot\vec{N}) + \kappa(\vec{\nabla}\times\vec{V}) - \gamma\vec{\nabla}\times(\vec{\nabla}\times\vec{V}) - 2\kappa\vec{N} \tag{3}$$

Current density vector:

$$\vec{J} = \sigma(\vec{E} + \vec{V}\times\vec{B}) - \frac{\omega_e\tau_e}{B}(\vec{J}\times\vec{B}) + \frac{\omega_e\tau_e\omega_i\tau_i}{B^2}(\vec{J}\times\vec{B})\times\vec{B} \tag{4}$$

Maxwell's equations:

$$div\vec{B} = 0 \tag{5a}$$

$$\vec{\nabla}\times\vec{H} = \vec{J} \tag{5b}$$

$$\vec{\nabla}\times\vec{E} = 0 \tag{5c}$$

Energy equation

$$\rho C_p(\vec{V}\cdot\vec{\nabla})T = \kappa\nabla^2 T + \Theta \tag{6}$$

Θ is energy loss function due to viscosity and Joule heating. Concentration equation:

$$\rho C_p(\vec{q}\cdot\vec{\nabla})C = D\nabla^2 C + \phi \tag{7}$$

ϕ is mass function due to chemical reaction.

To simplify the problem, the authors consider that there is no change in flow, heat transfer and mass transfer quantities in z-axis. The conservation of electric charge equation $\nabla J = 0$ implies J_y is constant. Since the wedge is non-conducting J_y is zero, everywhere in the flow. Also E_x is zero throughout the fluid. Further, it was considered that the induced magnetic field can be ignored in comparison to the applied magnetic field, whereas the combined effects of Joule heating and viscous dissipation are included.

The flow equations of the problem in Cartesian coordinates are as follows:

$$\frac{\partial u}{\partial x} + \frac{\partial v}{\partial y} = 0 \tag{8}$$

$$u\frac{\partial u}{\partial x}+v\frac{\partial u}{\partial y}=U\frac{\partial U}{\partial x}+\frac{\mu+\kappa}{\rho}\frac{\partial^2 u}{\partial y^2}+\frac{\kappa}{\rho}\frac{\partial N}{\partial y}+\frac{1}{\rho}\left(\frac{\sigma B_y^2}{\alpha_e^2+\beta_e^2}(\alpha_e(U-u)-\beta_e w)\right) \tag{9}$$

$$u\frac{\partial w}{\partial x}+v\frac{\partial w}{\partial y}=\frac{\mu+\kappa}{\rho}\frac{\partial^2 w}{\partial y^2}+\frac{\kappa}{\rho}\frac{\partial N}{\partial y}-\frac{1}{\rho}\left(\frac{\sigma B_y^2}{\alpha_e^2+\beta_e^2}(\alpha_e w-\beta_e u)\right) \tag{10}$$

$$u\frac{\partial N}{\partial x}+v\frac{\partial N}{\partial y}=\frac{\gamma_0}{\rho j}\frac{\partial^2 N}{\partial y^2}-\frac{\kappa}{\rho j}\left(2N+\frac{\partial u}{\partial y}\right) \tag{11}$$

$$\rho C_p\left(u\frac{\partial T}{\partial x}+v\frac{\partial T}{\partial y}\right)=k_0\frac{\partial^2 T}{\partial y^2}+(\mu+\kappa)\left(\left(\frac{\partial u}{\partial y}\right)^2+\left(\frac{\partial w}{\partial y}\right)^2\right)+\frac{\sigma B_y^2}{\alpha_e^2+\beta_e^2}(u^2+w^2)+Q_0(T-T_\infty) \tag{12}$$

$$u\frac{\partial C}{\partial x}+v\frac{\partial C}{\partial y}=D\frac{\partial^2 C}{\partial y^2}-R_0(C-C_\infty) \tag{13}$$

where $\alpha_e = 1+\beta_i\beta_e$, along (x,y,z) directions (u,v,w) are the velocity components. To find the problem similarity solutions, the variable magnetic field $B_y(x)$ is taken as the form $B_y=B_0x^{(m-1)/2}$ where, B_0 be the constant magnetic field. Further, we assumes that velocity for free stream be $U=ax^m$ [12], where a be a constant and m be the parameter of Falkner-Skan power-law, which is lies in $0 \le m \le 1$. Here $m=\beta/(2-\beta)$ where β is the parameter of Hartree pressure gradient which is equal to $\beta=\Omega/\pi$ for angle Ω of wedge. We observe that m is zero, for flow over a stationary plate and on an infinite wall flow near the stagnation point $m=1$. Further, N (component of microrotation), k_0 (thermal conductivity), μ (dynamic viscosity), κ (vortex viscosity), ρ (fluid density), T (temperature) of the fluid, Q_0 (heat source/sink constant), C_p (specific heat capacity) at constant pressure, D (mass diffusivity), C (concentration) of the fluid, R_0 (chemical reaction rate constant) and γ_0 (viscosity of spin gradient) expressed as $\gamma_0 = (\mu+0.5\kappa)j = \mu(1+0.5K)j$, where $K=\kappa/\mu$ is the micropolar or material parameter, $K=0$ corresponds to the classical equations of Navier-Stokes for incompressible and viscous fluid.

The governing boundary conditions for the flow are:

$$\left.\begin{aligned} &u=L\frac{\partial u}{\partial y},\quad v=v_w,\quad w=0,\quad N=-n\frac{\partial u}{\partial y},\\ &q_w=-k\frac{\partial T}{\partial y},\quad q_m=-D\frac{\partial C}{\partial y}\quad \text{at}\quad y=0,\\ &u\to U,\quad w\to 0,\quad N\to 0,\quad T\to T_0,\quad C\to C_0\quad \text{as}\quad y\to\infty \end{aligned}\right\} \tag{14}$$

Here L is the slip length, v_w is the uniform mass flux with, v_w is positive for suction and v_w is negative for blowing (injection), the constant term n range is [0, 1] ([19,20]).

Eqs. (8)–(13) can be transformed into a set of non-linear ODEs by applying the subsequent similarity transformations [19,20]:

$$\left.\begin{aligned} &\psi=\left(\frac{2xvU}{m+1}\right)^{1/2}f(\eta),\ N=\left(\frac{(m+1)U}{2xv}\right)^{1/2}Uh(\eta),\\ &w=Ug(\eta),\ \eta=\left(\frac{(m+1)U}{2xv}\right)^{1/2}y,\\ &\theta(\eta)=\frac{k(T-T_\infty)}{q_w}\left(\frac{(m+1)U}{2xv}\right)^{1/2},\\ &\phi(\eta)=\frac{D(C-C_\infty)}{q_m}\left(\frac{(m+1)U}{2xv}\right)^{1/2} \end{aligned}\right\} \tag{15}$$

The coupled systems of transformed nonlinear ordinary differential equations are:

$$(1+K)\frac{d^3f}{d\eta^3}+f\frac{d^2f}{d\eta^2}+\frac{2m}{1+m}\left(1-\left(\frac{df}{d\eta}\right)^2\right)+K\frac{\partial h}{\partial\eta}+\frac{M}{\alpha_e^2+\beta_e^2}\left(\alpha_e\left(1-\frac{df}{d\eta}\right)-\beta_e g\right)=0 \tag{16}$$

$$(1+K)\frac{d^2g}{d\eta^2}+f\frac{dg}{d\eta}-\left(\frac{2m}{1+m}\right)g\frac{df}{d\eta}-\frac{M}{\alpha_e^2+\beta_e^2}\left(\alpha_e g-\beta_e\frac{df}{d\eta}\right)=0 \tag{17}$$

$$\left(1+\frac{K}{2}\right)\frac{d^2h}{d\eta^2}-\left(\left(\frac{3m-1}{m+1}\right)\frac{df}{d\eta}h-f\frac{dh}{d\eta}\right)-\frac{2KI}{1+m}\left(2h+\frac{d^2f}{d\eta^2}\right)=0 \tag{18}$$

$$\left(\frac{1+m}{Pr}\right)\frac{d^2\theta}{d\eta^2}+(m+1)f\frac{d\theta}{d\eta}+(1+K)Ec\left(\left(\frac{d^2f}{d\eta^2}\right)^2+\left(\frac{dg}{d\eta}\right)^2\right)\theta+(m-1)\frac{df}{d\eta}\theta+\frac{EcM}{\alpha_e^2+\beta_e^2}\left(\left(\frac{df}{d\eta}\right)^2+g^2\right)\theta+H\theta=0 \tag{19}$$

$$\left(\frac{1+m}{Sc}\right)\frac{d^2\phi}{d\eta^2}+(m+1)f\frac{d\phi}{d\eta}+(m-1)\frac{df}{d\eta}\phi-\gamma\phi=0 \tag{20}$$

where ψ be stream function i.e. $u=\frac{\partial\psi}{\partial y}$ and $v=-\frac{\partial\psi}{\partial x}$. Further, $M=\frac{2\sigma B_0^2}{a\rho(1+m)}$ be magnetic parameter, $I=\frac{v^2Re}{jU^2}$ be inertia parameter, $Ec=\frac{U^2}{C_p(T-T_\infty)}$ be Eckert number, $Pr=\frac{\mu C_p}{k_0}$ be Prandtl number, $H=\frac{2xQ_0}{\rho C_pU}$ be local heat generation/absorption parameter, $Sc=\frac{v}{D}$ be Schmidt number, $\gamma=\frac{2xR_0}{U}$ be local chemical reaction parameter, $Re=\frac{xU}{v}$ be local Reynolds number.

The transformed boundary conditions in non-dimensional form are:

$$\left.\begin{aligned} &f(\eta)=F_w,\ \frac{df}{d\eta}=\delta\frac{d^2f}{d\eta^2},\ g(\eta)=0,\ h(\eta)=-(1-n)\frac{d^2f}{d\eta^2},\\ &\frac{d\theta}{d\eta}=-1,\ \frac{d\phi}{d\eta}=-1\ \text{at}\ \eta=0,\\ &\frac{df}{d\eta}\to 1,\ g(\eta)\to 0,\ h(\eta)\to 0,\\ &\theta(\eta)\to 0,\ \phi(\eta)\to 0\ \text{as}\ \eta\to\infty \end{aligned}\right\} \tag{21}$$

where, $F_w=-2\left(\frac{x(m+1)}{2vU}\right)^{1/2}v_w$ be the local suction/blowing parameter, $\delta=\left(\frac{(1+m)U}{2vx}\right)^{1/2}L$ be the local slip parameter.

The most important physical quantities for the problem are the (surface drag forces) (skin-friction coefficients) C_{fx} and C_{fz}, the local Nusselt number Nu and Sherwood number Sh, which are expressed as:

$$\begin{aligned} &C_{fx}=\frac{\tau_w}{\frac{1}{2}\rho U^2},\quad C_{fz}=\frac{\tau_z}{\frac{1}{2}\rho U^2},\quad Nu=\frac{xq_w}{k_0(T-T_\infty)},\\ &Sh=\frac{xm_w}{D(C-C_\infty)} \end{aligned} \tag{22}$$

where, the skin-frictions (surface drag forces) on the wedge surface τ_w and τ_z, rate of heat transfer q_w and rate of mass transfer m_w can be expressed as follows:

$$\left.\begin{aligned} &\tau_w=\left((\mu+\kappa)\frac{\partial u}{\partial y}+\kappa N\right)_{y=0},\quad \tau_z=\left((\mu+\kappa)\frac{\partial w}{\partial y}\right)_{y=0},\\ &q_w=-k_0\left(\frac{\partial T}{\partial y}\right)_{y=0},\quad m_w=-D\left(\frac{\partial C}{\partial y}\right)_{y=0} \end{aligned}\right\} \tag{23}$$

Using Eqs. (15) and (23) into Eq. (22) we have:

$$\left.\begin{aligned} &C_{fx}{}^*=Re^{1/2}C_{fx}=\sqrt{2(1+m)}\left(1+\frac{K}{2}\right)f''(0),\\ &C_{fz}{}^*=Re^{1/2}C_{fz}=\sqrt{2(1+m)}(1+K)g'(0),\\ &Nu^*=Re^{-1/2}Nu=\sqrt{\frac{1+m}{2}}\ \frac{1}{\theta(0)},\\ &Sh^*=Re^{-1/2}Sh=\sqrt{\frac{1+m}{2}}\ \frac{1}{\phi(0)} \end{aligned}\right\} \tag{24}$$

3. Differential transform method (DTM)

3.1. Basic idea

Let analytic function $f(\eta)$ is defined in a domain $\overline{T}$ and an arbitrary point within the domain is $\eta=\eta_0$. Now, at $\eta=\eta_0$ the DTM of $f(\eta)$ is written as (see Refs. [34,40]):

$$F[k]=\frac{1}{k!}\left[\frac{d^kf(\eta)}{d\eta^k}\right]_{\eta\ =\ \eta_0} \tag{25}$$

where, the converted function $F[k]$ which is usually known as the $\overline{T}$-function. Now, the inverse formulation for DTM is established as:

$$f(\eta)=\sum_{k=0}^{\infty}\frac{F[k]}{(\eta-\eta_0)^{-k}} \tag{26}$$

Combining Eqs. (25) and (26) then we get:

$$f(\eta)=\sum_{k=0}^{\infty}\frac{(\eta-\eta_0)^k}{k!}\left[\frac{d^kf(\eta)}{d\eta^k}\right]_{\eta\ =\ \eta_0} \tag{27}$$

actually $f(\eta)$ is defined as:

$$f(\eta)=\sum_{k=0}^{Z}\frac{F[k]}{(\eta-\eta_0)^{-k}} \tag{28}$$

which, means that $f(\eta)=\sum_{k=N+1}^{\infty}(\eta-\eta_0)^kF[k]$ is negligibly small. Usually, the value of Z is decided by series coefficients of convergence. Now applying Eqs. (25)–(28) and some basic operations of differential transformation method, the following consequence of the problem can be derived.

3.2. DTM implementation

Applying DTM in Eq. (16) and we obtained the following:

$$(1+K)(k+1)(k+2)(k+3)F[k+3]=$$
$$-\sum_{l=0}^{k}F(l)(k-l+1)\big(k-l+2\big)F\big(k-l+2\big)$$
$$-\frac{2m}{1+m}\left(1-\sum_{l=0}^{k}(l+1)F(l+1)(k-l+1)F\big(k-l+1\big)\right)$$
$$-KH\big[k\big]-\frac{M}{\alpha_e^2+\beta_e^2}(\alpha_e(1-(k+1)F[k+1])-\beta_e G[k]) \tag{29}$$

The associated boundary conditions are transformed into:

$$F[0]=F_w,\ F[1]=\delta\alpha_1,\ F[2]=\alpha_1 \tag{30}$$

Further, using the DTM method in Eq. (17) and we get:

$$(1+K)(k+1)(k+2)G[k+2]=$$
$$-\sum_{l=0}^{k}F[l](k-l+1)G(k-l+1)$$
$$+\left(\frac{2m}{1+m}\right)\sum_{l=0}^{k}G[l](k-l+1)F(k-l+1)$$
$$+\frac{M}{\alpha_e^2+\beta_e^2}(\alpha_e G[k]-\beta_e(k+1)F[k+1]) \tag{31}$$

Now, the boundary conditions are altered into

$$G[0]=0,\ G[1]=\alpha_2 \tag{32}$$

Further, applying the DTM in Eq. (18) and we get:

$$\left(1+\frac{K}{2}\right)(k+1)(k+2)H[k+2]=$$
$$\left(\frac{3m-1}{m+1}\right)\sum_{l=0}^{k}(l+1)F[l+1]H[k-l]$$
$$-\sum_{l=0}^{k}F[l](k-l+1)H[k-l+1] \tag{33}$$
$$+\frac{2KI}{1+m}(2H[k]+(k+1)(k+2)F[k+2])$$

The related boundary conditions are also changed, it can be written as:

$$H[0]=-0.5\alpha_1,\ H[1]=\alpha_3 \tag{34}$$

Making use of DTM in Eq. (19) we obtained:

$$\left(\frac{1+m}{Pr}\right)(k+1)(k+2)\Theta[k+2]=$$
$$-(m+1)\sum_{l=0}^{k}F[l](k-l+1)\Theta[k-l+1]-(m-1)\sum_{l=0}^{k}(l+1)\times F[l+1]\Theta[k-l]$$
$$-(1+K)Ec\times\left(\sum_{l=0}^{k}\sum_{r=0}^{k-l}(l+1)(l+2)F[l+2](r+1)(r+2)F[r+2]\Theta[k-l-r]\right)$$
$$-(1+K)Ec\times\left(\sum_{l=0}^{k}\sum_{r=0}^{k-l}(l+1)G[l+1](r+1)G[r+1]\Theta[k-l-r]\right)$$
$$-\frac{EcM}{\alpha_e^2+\beta_e^2}\left(\sum_{l=0}^{k}\sum_{r=0}^{k-l}G[l]G[r]\Theta[k-l-r]\right)-\frac{EcM}{\alpha_e^2+\beta_e^2}\left(\sum_{l=0}^{k}\sum_{r=0}^{k-l}(l+1)F[l+1](r+1)F[r+1]\Theta[k-l-r]\right)-H\Theta[k] \tag{35}$$

The transformed boundary conditions are:

$$\Theta[0]=\alpha_4,\ \Theta[1]=-1. \tag{36}$$

Now, applying the DTM in Eq. (20) we get:

$$\left(\frac{1+m}{Sc}\right)(k+1)(k+2)\Phi[k+2]=$$
$$-(m+1)\sum_{l=0}^{k}F[l](k-l+1)\Phi[k-l+1]$$
$$-(m-1)\sum_{l=0}^{k}(l+1)F[l+1]\Phi[k-l]+\gamma\Phi[k] \quad (37)$$

The governing boundary conditions are reduced into:

$$\Phi[0]=\alpha_5,\ \Phi[1]=-1. \quad (38)$$

By solving these above equations, we achieved:

$$F[3]=\frac{1}{6(1+K)}\times$$
$$\left(-2F_w\alpha_1-\frac{2m}{1+m}\left(1-(\delta\alpha_1)^2\right)+\frac{K\alpha_1}{2}-\frac{M\alpha_e}{\alpha_e^2+\beta_e^2}(1-\delta\alpha_1)\right),$$

$$F[4]=\frac{F_w}{24(1+K)^2}\left(2F_w\alpha_1+\frac{2m}{1+m}\left(1-(\delta\alpha_1)^2\right)\right)$$
$$-\frac{F_w}{24(1+K)^2}\left(\frac{K\alpha_1}{2}-\frac{M\alpha_e}{\alpha_e^2+\beta_e^2}(1-\delta\alpha_1)\right)$$
$$+\frac{1}{24(1+K)}\left(-\frac{2m}{(1+m)}\left(1-4\delta F_w{\alpha_1}^2\right)-2\delta\alpha_1^2-K\alpha_3\right)$$
$$+\frac{1}{24(1+K)}\left(-\frac{M}{\alpha_e^2+\beta_e^2}(\alpha_e(1-2\alpha_1)-\beta_e\alpha_2)\right),\ldots \quad (39)$$

$$G[2]=\frac{1}{2(1+K)}\left(-F_w\alpha_2+\frac{M\beta_e}{\alpha_e^2+\beta_e^2}\delta\alpha_1\right),$$

$$G[3]=\frac{1}{6(1+K)}\left[\frac{F_w}{(1+K)}\left(F_w\alpha_2-\frac{M\beta_e}{\alpha_e^2+\beta_e^2}\delta\alpha_1\right)\right]$$
$$+\frac{1}{6(1+K)}\left(\frac{m-1}{1+m}\delta\alpha_1\alpha_2+\frac{M}{\alpha_e^2+\beta_e^2}(\alpha_e\alpha_2-2\beta_e\alpha_1)\right),\ldots \quad (40)$$

$$H[2]=\frac{1}{(2+K)}\left[-\frac{1}{2}\left(\frac{3m-1}{m+1}\right)\delta\alpha_1^2-F_w\alpha_3+\frac{2KI}{1+m}\alpha_1\right],$$

$$H[3]=\frac{1}{3(2+K)}\left[\frac{2(m-1)}{m+1}\delta\alpha_1\alpha_3\right]$$
$$+\frac{1}{3(2+K)}\left[-\frac{2F_w}{(2+K)}\left(-\frac{1}{2}\left(\frac{3m-1}{m+1}\right)\delta\alpha_1^2\right.\right.$$
$$\left.\left.-F_w\alpha_3+\frac{2KI}{1+m}\alpha_1\right)\right]-\frac{1}{3(2+K)}\left(\frac{3m-1}{m+1}\right)\alpha_1^2$$
$$+\frac{4KI}{3(2+K)(m+1)}\alpha_3+\frac{2KI}{3(2+K)(m+1)}\times\left(\frac{1}{(1+K)}\times\right.$$
$$\left.\left(-2F_w\alpha_1-\frac{2m}{1+m}\left(1-\delta^2{\alpha_1}^2\right)+\frac{K\alpha_1}{2}-\frac{M\alpha_e}{\alpha_e^2+\beta_e^2}(1-\delta\alpha_1)\right)\right) \quad (41)$$

$$\Theta[2]=-\frac{Pr\alpha_4}{2(1+m)}\left((m-1)\delta\alpha_1-(1+K)Ec\left(4{\alpha_1}^2+{\alpha_2}^2\right)\right.$$
$$\left.+\frac{EcM}{\alpha_e^2+\beta_e^2}(\delta\alpha_1)^2+H\right)+\frac{Pr}{2(1+m)}(m+1)F_w,\ldots \quad (42)$$

$$\Phi[2]=\frac{Sc}{2(1+m)}[(m+1)F_w-(m-1)\delta\alpha_1\alpha_5+\gamma\alpha_5],$$

$$\Phi[3]=\frac{-Sc}{6(1+m)}\times$$
$$\left[\begin{array}{l}(1+m)\left(\frac{ScF_w}{(1+m)}[(m+1)F_w-(m-1)\delta\alpha_1\alpha_5+\gamma\alpha_5]\right)\\+(m-1)(-\delta\alpha_1+2\alpha_1\alpha_5)+\gamma\end{array}\right],\ldots \quad (43)$$

Putting the above outcomes in the basic equation of DTM, we acquired the expression for $f(\eta)$, $g(\eta)$, $h(\eta)$, $\theta(\eta)$ and $\phi(\eta)$ given below:

$$f(\eta)=F_w+\delta\alpha_1\eta+\alpha_1\eta^2$$
$$+\frac{1}{6(1+K)}\left[-2F_w\alpha_1-\frac{2m}{1+m}\left(1-(\delta\alpha_1)^2\right)+\frac{K\alpha_1}{2}-\frac{M\alpha_e}{\alpha_e^2+\beta_e^2}(1-\delta\alpha_1)\right]\eta^3$$
$$+\left[\begin{array}{l}\frac{1}{24(1+K)}\left(-\frac{F_w}{(1+K)}\left(-2F_w\alpha_1-\frac{2m}{1+m}\left(1-(\delta\alpha_1)^2\right)\right)\right)\\+\frac{1}{24(1+K)}\left(-\frac{F_w}{(1+K)}\left(\frac{K\alpha_1}{2}-\frac{M\alpha_e}{\alpha_e^2+\beta_e^2}(1-\delta\alpha_1)\right)\right)\\+\frac{1}{24(1+K)}\left(\frac{-2m}{(1+m)}\left(1-4\delta F_w{\alpha_1}^2\right)-2\delta\alpha_1^2-K\alpha_3\right)\\-\frac{1}{24(1+K)}\frac{M}{\alpha_e^2+\beta_e^2}(\alpha_e(1-2\alpha_1)-\beta_e\alpha_2)\end{array}\right]\eta^4+\ \ldots \quad (44)$$

$$g(\eta)=\alpha_2\eta+\frac{1}{2(1+K)}\left(-F_w\alpha_2+\frac{M\beta_e}{\alpha_e^2+\beta_e^2}\delta\alpha_1\right)\eta^2 \\ +\frac{1}{6(1+K)}\left[\begin{array}{l}\frac{F_w}{(1+K)}\left(F_w\alpha_2-\frac{M\beta_e}{\alpha_e^2+\beta_e^2}\delta\alpha_1\right)\\ +\frac{m-1}{1+m}\delta\alpha_1\alpha_2\\ +\frac{M}{\alpha_e^2+\beta_e^2}(\alpha_e\alpha_2-2\beta_e\alpha_1)\end{array}\right]\eta^3+\ldots\Bigg\} \tag{45}$$

4. Results and discussion

In order to assess the impacts of various pertinent parameters on the flow, numerical simulations are performed for the range $0\le\delta\le1$, $-0.4\le H\le0.4$, $0.5\le Sc\le2$ and $0\le\gamma\le1$ while $I=0.5=Ec$, $Pr=1=M$, $\beta_e=2$ and $\beta_i=0.4$ are fixed and authors take $n=1/2$ (weak concentration). To confirm the validity of obtained analytic outcomes, authors compared current data with earlier published study as depicted in Table 1, we got an excellent agreement.

Figures 2–4 show the velocities profiles due unlike values of slip parameter δ and suction/injection parameter F_w. It is found from Figure 2 that an increment in the values of δ and F_w cause an increase in horizontal velocity $f'(\eta)$. It is clear from Figure 3 that the transverse velocity $g(\eta)$ accelerates close to the surface of wedge while a reverse trend

$$h(\eta)=-0.5\alpha_1+\alpha_3\eta+\frac{1}{(2+K)}\left[-\frac{1}{2}\left(\frac{3m-1}{m+1}\right)\delta\alpha_1^2-F_w\alpha_3+\frac{2KI}{1+m}\alpha_1\right]\eta^2 \\ +\frac{1}{3(2+K)}\left[\begin{array}{l}\frac{2(m-1)}{m+1}\delta\alpha_1\alpha_3-\left(\frac{3m-1}{m+1}\right)\alpha_1^2+\frac{4KI\alpha_3}{m+1}\\ -\frac{2F_w}{(2+K)}\left(-\frac{1}{2}\left(\frac{3m-1}{m+1}\right)\delta\alpha_1^2-F_w\alpha_3+\frac{2KI}{1+m}\alpha_1\right)\\ +\frac{2KI}{m+1}\times\left(\frac{1}{(1+K)}\left(-2F_w\alpha_1-\frac{2m}{1+m}\left(1-\delta^2{\alpha_1}^2\right)+\frac{K\alpha_1}{2}-\frac{M\alpha_e}{\alpha_e^2+\beta_e^2}(1-\delta\alpha_1)\right)\right)\end{array}\right]\eta^3+\ldots\Bigg\} \tag{46}$$

$$\theta(\eta)=\alpha_4-\eta+\frac{Pr}{2(1+m)}\left[\begin{array}{l}\left((m-1)\delta\alpha_1-(1+K)Ec\left(4{\alpha_1}^2+{\alpha_2}^2\right)\right)\alpha_4\\ +\frac{EcM}{\alpha_e^2+\beta_e^2}(\delta\alpha_1)^2+H\\ +(m+1)F_w\end{array}\right]\eta^2+\ldots\Bigg\} \tag{47}$$

$$\phi(\eta)=\alpha_5-\eta+\frac{Sc}{2(1+m)}[(m+1)F_w-(m-1)\delta\alpha_1\alpha_5+\gamma\alpha_5]\eta^2 \\ +\frac{Sc}{6(1+m)}\left[\begin{array}{l}-(1+m)\left(\frac{ScF_w}{(1+m)}[(m+1)F_w-(m-1)\delta\alpha_1\alpha_5+\gamma\alpha_5]\right)\\ -(m-1)(-\delta\alpha_1+2\alpha_1\alpha_5)-\gamma\end{array}\right]\eta^3+\ldots \tag{48}$$

Now, by comparing Eqs. (44)–(48) at $\eta=\infty$ (we take $\eta=3$ in large sense of η) with boundary conditions Eq. (21). Then α_1, α_2, α_3, α_4 and α_5 are obtained. By substituting these values of α_1, α_2, α_3, α_4 and α_5 in Eqs. (44)–(48), we have derived the expressions for $f(\eta)$, $g(\eta)$, $h(\eta)$, $\theta(\eta)$ and $\phi(\eta)$.

Table 1 Comparison of $C_{fx}Re^{1/2}$ values as m varies, when $\beta_i=0.4$, $\beta_e=0$, $K=0$, $M=0$, $I=0.5$, $Ec=0$, $\delta=0$, $H=0$, $Sc=0$ and $\gamma=0$.

m	Yih [8]	Ishak et al. [6]	Uddin & Kumar [19]	Present results
0	0.332057	0.3321	0.3466	0.34528
1/3	0.757448	0.7575	0.7586	0.75836
1	1.232588	1.2326	1.2328	1.23254

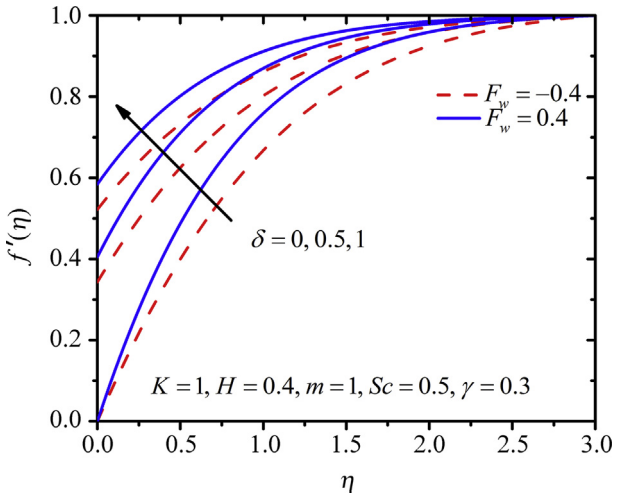

Figure 2 Effects of δ and F_w on $f'(\eta)$.

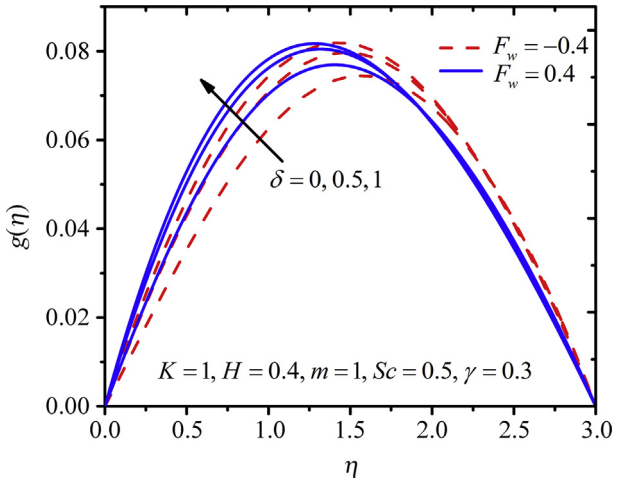

Figure 3 Effects of δ and F_w on $g(\eta)$.

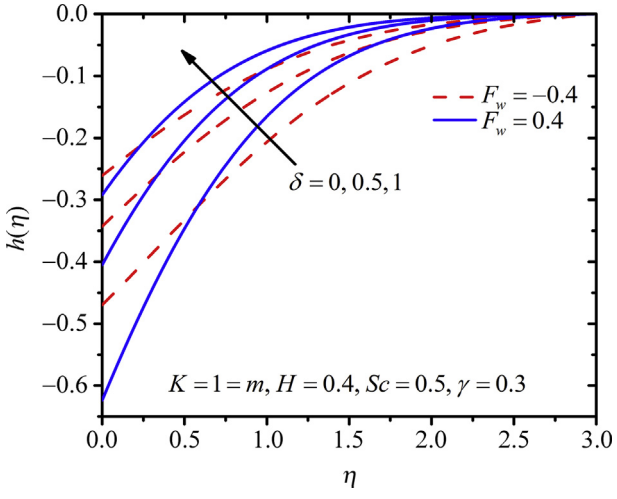

Figure 4 Effects of δ and F_w on $h(\eta)$.

is seen near free stream when δ and F_w increases. Figure 4 indicates that the angular velocity $h(\eta)$ clearly increase as δ and F_w rises.

The influences of heat generation/absorption parameter H, slip parameter δ and suction/injection parameter F_w on $\theta(\eta)$ are depicted in Figures 5 and 7. It is observed that, by growing either value of δ, H or F_w, the dimensionless temperature curve decreases.

In Figures 6, 8 and 9, the impacts of parameters δ, Sc, γ and F_w on the dimensionless concentration $\phi(\eta)$ are displayed. The concentration profiles $\phi(\eta)$ decreases markedly with the escalating values of δ, Sc, γ and F_w.

The variation of the skin-friction coefficient (surface drag force) $C_{fx}{}^*$ is depicted for different parameters in Figures 10 and 11. Figure 10 illustrates the behaviour of the skin friction coefficient $C_{fx}{}^*$ against suction/injection parameter F_w with various values of the slip parameter δ and pressure gradient parameter m. The surface drag force $C_{fx}{}^*$ declines with grow in the slip parameter δ, while it augments as boost

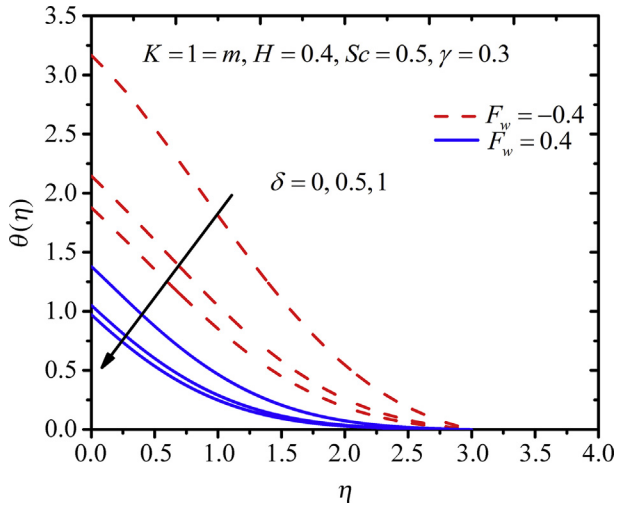

Figure 5 Effects of δ and F_w on $\theta(\eta)$.

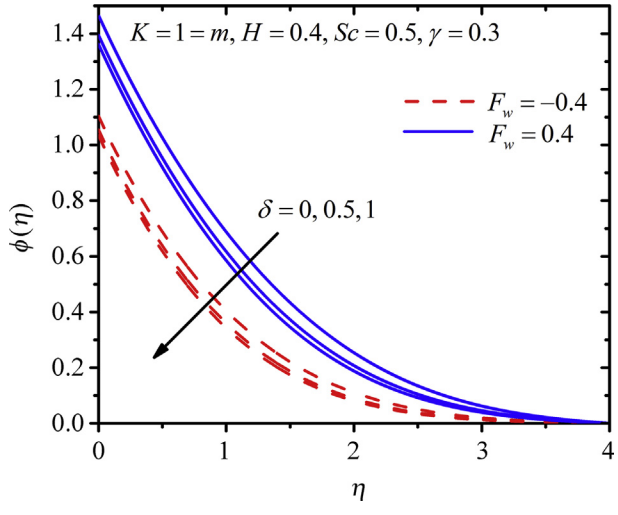

Figure 6 Effects of δ and F_w on $\phi(\eta)$.

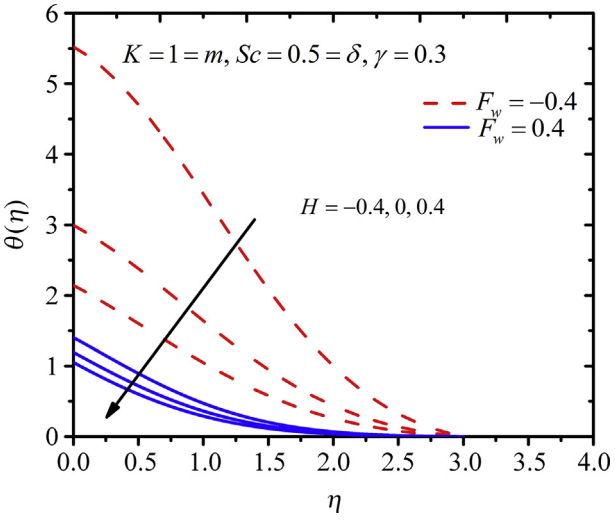

Figure 7 Effects of H and F_w on $\theta(\eta)$.

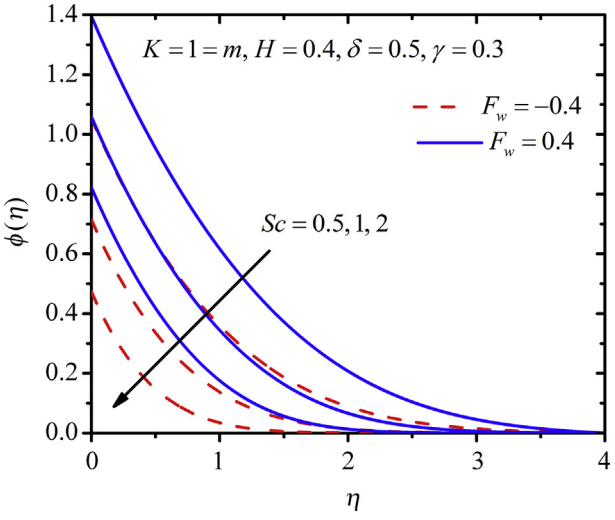

Figure 8 Effects of Sc and F_w on $\phi(\eta)$.

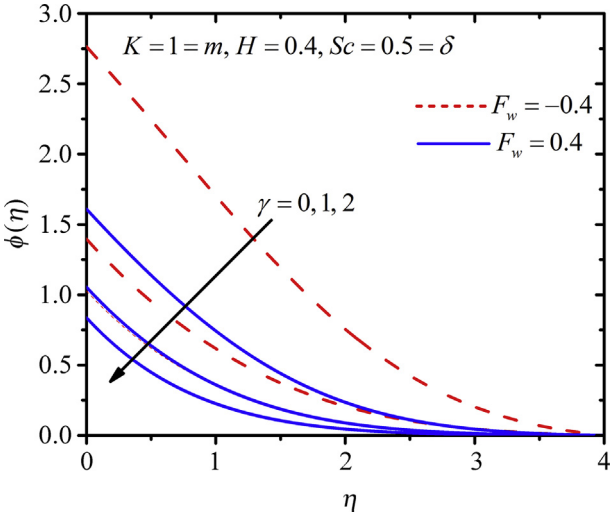

Figure 9 Effects of γ and F_w on $\phi(\eta)$.

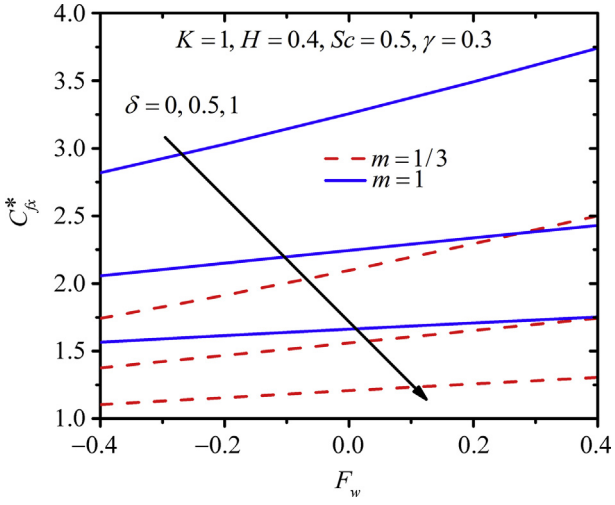

Figure 10 Variation in $C_{fx}{}^*$ with F_w, δ and m.

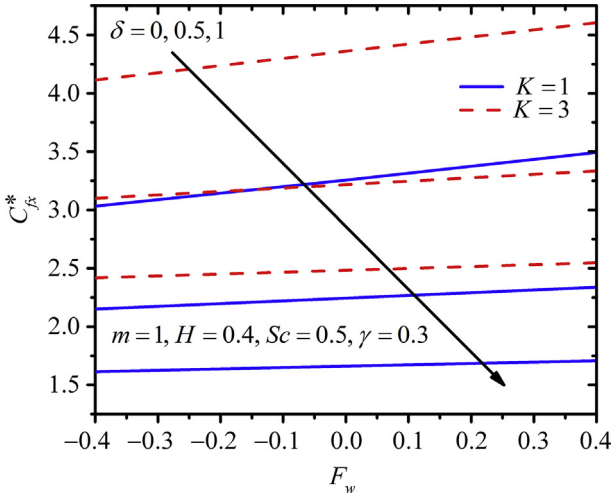

Figure 11 Variation in $C_{fx}{}^*$ with F_w, δ and K.

in F_w. Figure 11 demonstrates the discrepancy of $C_{fx}{}^*$ relating to the suction/injection parameter F_w, slip parameter δ and micro-polar or material parameter K. It is noticed that the surface drag force $C_{fx}{}^*$ monotonically decreases with a rise in δ, while same increases with increasing F_w.

Figure 12 depicts the deviation of the skin friction coefficient (surface drag force) $C_{fz}{}^*$ as a function of F_w for unlike values of δ and m. We observed from this figure that the upshot of rising F_w and δ is to add to skin friction coefficient (surface drag force) $C_{fz}{}^*$. The influence of F_w, δ and K on the surface drag force $C_{fz}{}^*$ are presented in Figure 13. It is seen that the surface drag force $C_{fz}{}^*$ monotonically increases with a rise in F_w and δ.

The graphs of Nusselt number (at surface dimensionless rate of heat transfer) Nu^* against F_w for altered values of δ, m and K are exposed in Figures 14 and 15. It is noted from these figures that the heat transfer rate rises significantly for large values of δ and F_w.

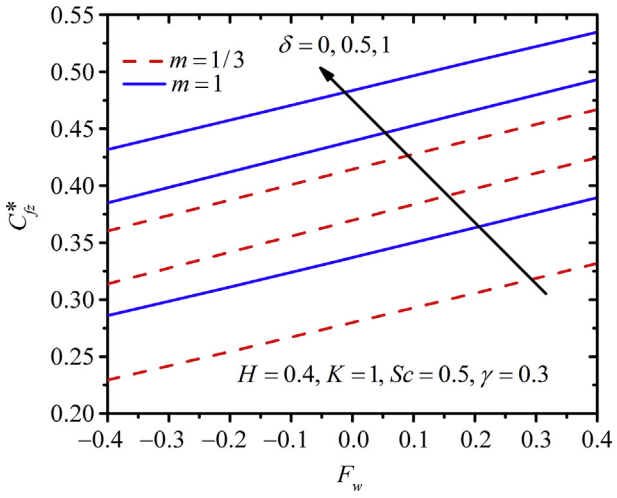

Figure 12 Variation in C_{fz}^* with F_w, δ and m.

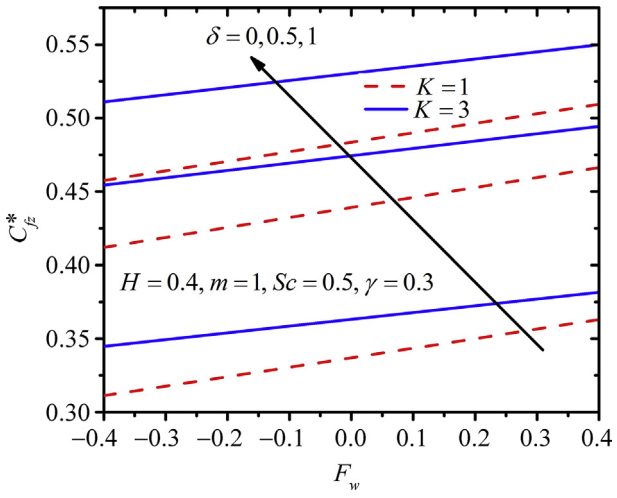

Figure 13 Variation in C_{fz}^* with F_w, δ and K.

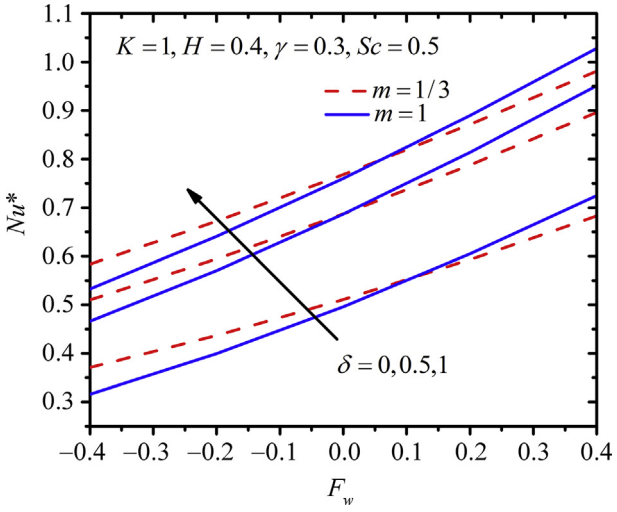

Figure 14 Variation in Nu^* with F_w, δ and m.

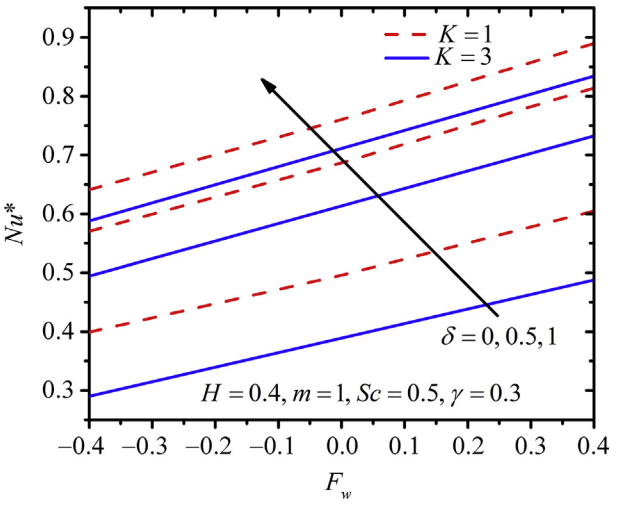

Figure 15 Variation in Nu^* with F_w, δ and K.

Figure 16 explores the variation of the Sherwood number (dimensionless mass transfer rate at surface) Sh^* with respect to F_w, δ and m. From this figure, it is detected that by increasing δ and F_w there is remarkable increase in the mass transfer rate.

The profile of the rate of mass transfer against F_w for diverse values of δ and K are exhibited in Figure 17. On seeing Figure 17 we noted that there is an enhancement in mass transfer rate with enhance in δ and F_w.

Figure 18 describes the effect of parameter H, the pressure gradient parameter m and the suction/injection parameter F_w on the local Nusselt number Nu^*. It is evident from Figure 18 that the effect of increasing H and F_w on the Nusselt number is to increase its value. Figure 19 depicts that when there is change in H values, the micropolar parameter K and the suction/injection parameter F_w, Nusselt number changes. From this figure, we scrutinized that the Nusselt number rise with ever-increasing the values of H and F_w.

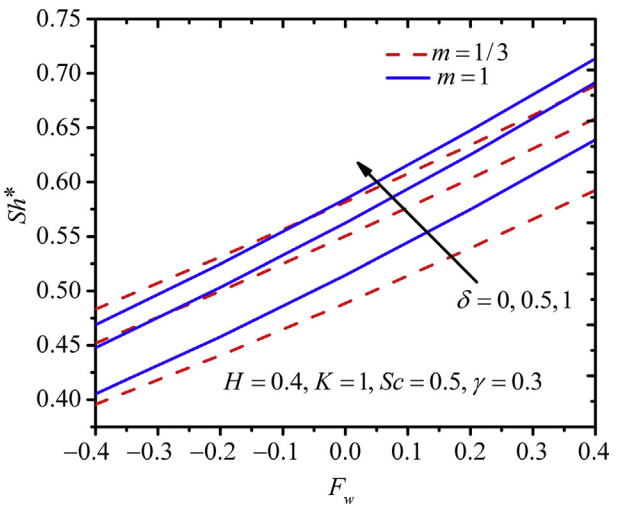

Figure 16 Variation in Sh^* with F_w, δ and m.

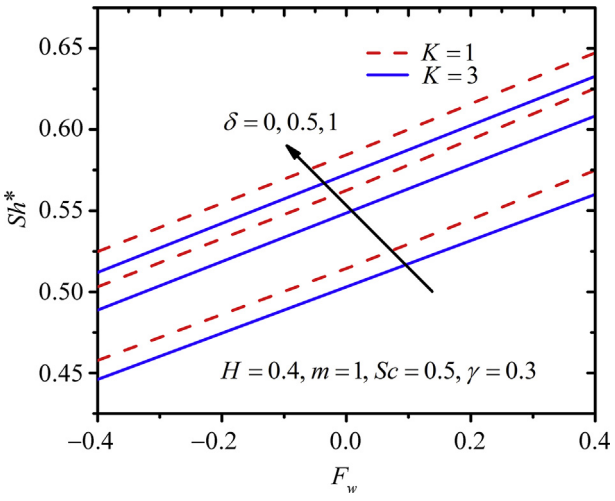

Figure 17 Variation in Sh^* with F_w, δ and K.

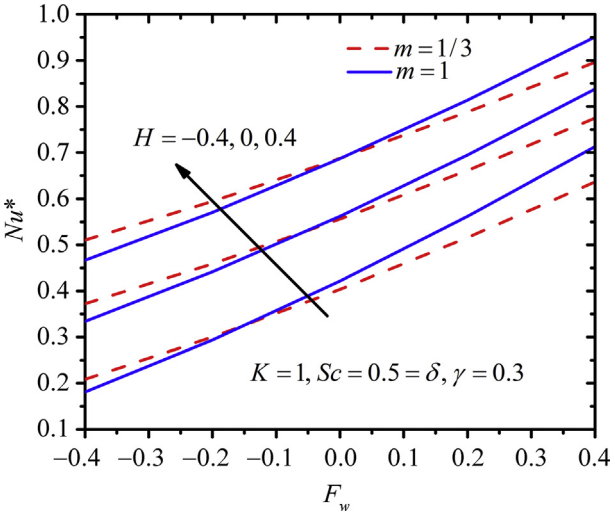

Figure 18 Variation in Nu^* with F_w, H and m.

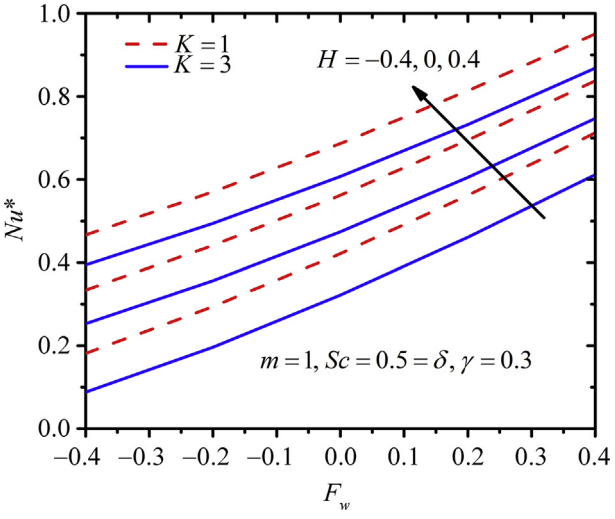

Figure 19 Variation in Nu^* with F_w, H and K.

Figures 20–21 display the deviation in Sherwood number (at the surface, rate of mass transfer) Sh^* against F_w for a choice of values of the Sc, the pressure gradient parameter m and the micropolar parameter K. From these figures, it is noted that rate of mass transfer reduces with escalate in Sc. Further, it is observed from Figures 20–21 that there is a constant boost in the mass transfer rate as an augment in F_w and the rate of increase become rapid for high values of F_w.

The plot of the Sherwood number (the rate of mass transfer at surface) against F_w for different value of γ and m are shown in Figure 22 and the variation of the same number against F_w for different value of γ and K are illustrated in Figure 23. We observe that the mass transfer rate monotonically increases as there is increase in γ and the suction/injection parameter F_w.

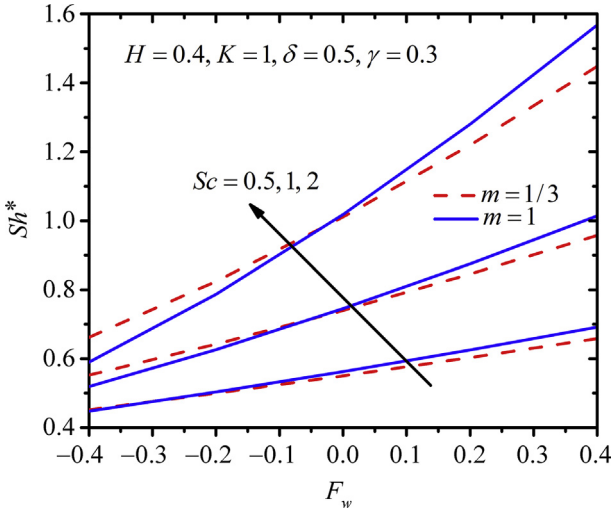

Figure 20 Variation in Sh^* with F_w, Sc and m.

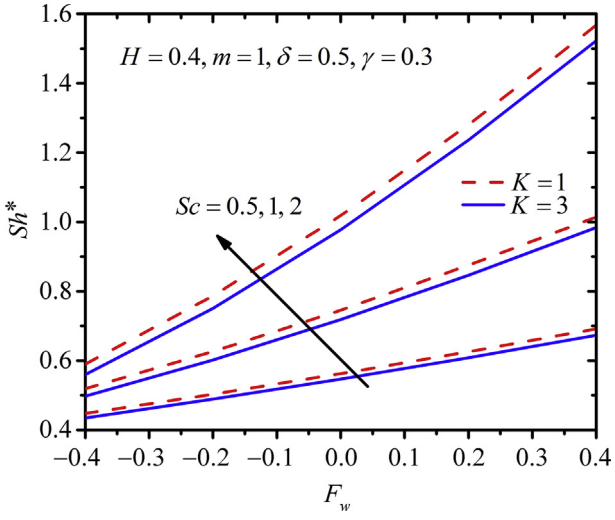

Figure 21 Variation in Sh^* with F_w, Sc and K.

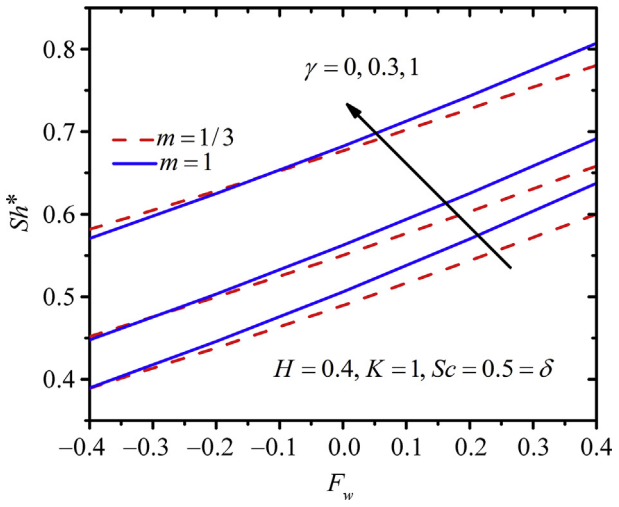

Figure 22 Variation in Sh^* with F_w, γ and m.

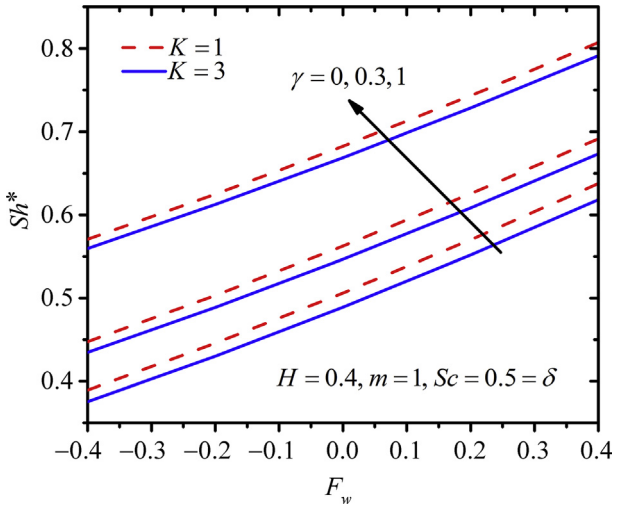

Figure 23 Variation in Sh^* with F_w, γ and K.

From the table, we observe that on escalating in K and m, $C_{fx}{}^*$ is enhances, while increasing in δ reduces $C_{fx}{}^*$ values. Moreover, the values of $C_{fz}{}^*$ exceeded as K, m and δ increases. Further, from Table 2 one can note that the Nusselt number Nu^* augments on growing the values of K and m, while declines as amplify the values of δ and H. It is also seen from Table 2 that the values of Sh^* increases on increasing values of m, δ, Sc and γ, but the Sherwood number decreases as K increases.

5. Conclusions

An analytical approach on steady flow through a permeable wedge is studied along with the impact of pertinent parameters chemical reaction, slip velocity and heat source/sink. By utilizing differential transformation method (DTM), the transformed equations are handled. In context to the above study, the outcomes of the present study have been described below:

- Increasing the slip and suction/injection parameter increases the horizontal and angular velocity.
- The temperature profiles are decreases by increasing slip, heat source/sink and suction/injection parameters.
- On mounting the values of relevant parameters i.e. slip parameter δ, Schmidt number Sc, chemical reaction parameter and suction/injection parameter F_w concentration curves are continuously depreciated.
- Surface drag force $C_{fx}{}^*$ augments as boost in the value of δ, while differing trend is noticed on $C_{fz}{}^*$.
- The heat transfer rate increases with increase in the slip and heat source/sink parameters.
- With increase in Schmidt number Sc, slip parameter δ and chemical reaction parameter, mass transfer rate enhances.

Table 2 Values of $C_{fx}{}^*$, $C_{fz}{}^*$, Nu^* and Sh^* with various values of parameters when $F_w = 0.4$.

K	m	δ	H	Sc	γ	$C_{fx}{}^*$	$C_{fz}{}^*$	Nu^*	Sh^*
1	1	0.5	0.4	0.5	0.3	2.42985	0.49316	0.951022	0.691611
3	1	0.5	0.4	0.5	0.3	3.45135	0.51448	0.868432	0.673491
1	1/3	0.5	0.4	0.5	0.3	1.743309	0.21229	1.097574	0.658415
1	1	0	0.4	0.5	0.3	3.74100	0.38940	0.724795	0.639059
1	1	1	0.4	0.5	0.3	1.75230	0.53480	1.027961	0.713572
1	1	0.5	−0.4	0.5	0.3	2.42985	0.49316	0.712911	0.691611
1	1	0.5	0	0.5	0.3	2.42985	0.49316	0.838082	0.691611
1	1	0.5	0.4	1	0.3	2.42985	0.49316	0.951022	1.014199
1	1	0.5	0.4	2	0.3	2.42985	0.49316	0.951022	1.567890
1	1	0.5	0.4	0.5	0	2.42979	0.49320	0.951113	0.637633
1	1	0.5	0.4	0.5	1	2.42979	0.49320	0.951113	0.807103

Table 2 depicts the disparity in surface drag forces ($C_{fx}{}^*$ and $C_{fz}{}^*$), Nusselt number Nu^* as well as Sh^* for a range of values of pertinent parameters.

Acknowledgements

The authors wish to convey their genuine gratitude to the reviewers for their essential suggestions and comments to

improve the quality of this manuscript. This research did not receive any specific grant.

References

[1] A.C. Eringen, Theory of micropolar fluid, J. Math. Mech. 16 (1966) 1−18.

[2] A.C. Eringen, Theory of thermomicrofluids, J. Math. Anal. Appl. 38 (1972) 480−496.

[3] E.M.A. Elbashbeshy, M.F. Dimian, Effect of radiation on the flow and heat transfer over a wedge with variable viscosity, Appl. Math. Comput. 132 (2002) 445−454.

[4] M. Xenos, E. Tzirtzilakis, N. Kafoussias, Methods of optimizing separation of compressible turbulent boundary-layer over a wedge with heat and mass transfer, Int. J. Heat Mass Tran. 52 (1−2) (2009) 488−496.

[5] P.J. Singh, S. Roy, R. Ravindran, Unsteady mixed convection flow over a vertical wedge, Int. J. Heat Mass Tran. 52 (1−2) (2009) 415−421.

[6] A. Ishak, R. Nazar, I. Pop, MHD boundary layer flow of a micropolar fluid past a wedge with constant wall heat flux, Commun. Nonlinear Sci. Numer. Simulat. 14 (2009) 109−118.

[7] M.M. Rahman, I.A. Eltayeb, Convective slip flow of rarefied fluids over a wedge with thermal jump and variable transport properties, Int. J. Therm. Sci. 50 (2011) 468−479.

[8] K.A. Yih, MHD forced convection flow adjacent to a non-isothermal wedge, Int. Commun. Heat Mass Tran. 26 (1999) 819−827.

[9] K. Hsiao, MHD mixed convection for viscoelastic fluid past a porous wedge, Int. J. Non Lin. Mech. 46 (2011) 1−8.

[10] F. Hedayati, A. Malvandi, D.D. Ganji, Second-law analysis of fluid flow over an isothermal moving wedge, Alexandria Eng. J. 53 (2014) 1−9.

[11] K. Vajravelu, S. Mukhopadhyay, Fluid Flow, Heat and Mass Transfer at Bodies of Different Shapes: Numerical Solutions, Academic Press, 2015.

[12] A.K. Pandey, M. Kumar, Effect of viscous dissipation and suction/injection on MHD nanofluid flow over a wedge with porous medium and slip, Alexandria Eng. J. 55 (4) (2016) 3115−3123.

[13] A.K. Pandey, M. Kumar, Chemical reaction and thermal radiation effects on boundary layer flow of nanofluid over a wedge with viscous and Ohmic dissipation, St. Petersburg Polytech. Univ. J. Phys. Math. 3 (4) (2017) 322−332.

[14] A.K. Pandey, M. Kumar, MHD flow inside a stretching/shrinking convergent/divergent channel with heat generation/absorption and viscous-Ohmic dissipation utilizing Cu-water nanofluid, Comput. Therm. Sci. 10 (5) (2019) 457−471.

[15] H. Upreti, A.K. Pandey, M. Kumar, MHD flow of Ag-water nanofluid over a flat porous plate with viscous-Ohmic dissipation, suction/injection and heat generation/absorption, Alexandria Eng. J. 57 (3) (2017) 1839−1847.

[16] A.M. Salem, M. Abd El-Aziz, Effect of Hall currents and chemical reaction on hydromagneticb flow of a stretching vertical surface with internal heat generation/absorption, Appl. Math. Model. 32 (2008) 1236−1254.

[17] N.S. Elgazery, The effects of chemical reaction, Hall and ion-slip currents on MHD flow with temperature dependent viscosity and thermal diffusivity, Commun. Nonlinear Sci. Numer. Simulat. 14 (2009) 1267−1283.

[18] D. Srinivasacharya, K. Kaladhar, Mixed convection flow of couple stress fluid between parallel vertical plates with Hall and Ion-slip effects, Commun. Nonlinear Sci. Numer. Simulat. 17 (2012) 2447−2462.

[19] Z. Uddin, M. Kumar, Hall and ion-slip effect on MHD boundary layer flow of a micropolar fluid past a wedge, Sci. Iran. B 20 (3) (2013) 467−476.

[20] Z. Uddin, M. Kumar, S. Harmand, Influence of thermal radiation and heat generation/absorption on MHD heat transfer flow of a micropolar fluid past a wedge with Hall and ion slip currents, Therm. Sci. 18 (2) (2014) S489−S502.

[21] D. Srinivasacharya, Ch RamReddy, P. Naveen, O. Surender, Non-Darcy mixed convection flow past a vertical porous plate with Joule heating, Hall and ion-slip effects, Process Eng. 127 (2015) 162−169.

[22] S.A. Gaffar, V.R. Prasad, E.K. Reddy, MHD free convection flow of Eyring-Powell fluid from vertical surface in porous media with Hall/ion slip currents and Ohmic dissipation, Alexandria Eng. J. 55 (2016) 875−905.

[23] A.A. Bakr, Effects of chemical reaction on MHD free convection and mass transfer flow of a micropolar fluid with oscillatory plate velocity and constant heat source in a rotating frame of reference, Commun. Nonlinear Sci. Numer. Simulat. 16 (2011) 698−710.

[24] A.M. Rashad, S. Abbasbandy, A.J. Chamkha, Mixed convection flow of a micropolar fluid over a continuously moving vertical surface immersed in a thermally and solutally stratified medium with chemical reaction, J. Taiwan Inst. Chem. Eng. 45 (2014) 2163−2169.

[25] F. Mabood, W.A. Khan, A.I.Md Ismail, MHD stagnation point flow and heat transfer impinging on stretching sheet with chemical reaction and transpiration, Chem. Eng. J. 273 (2015) 430−437.

[26] F. Mabood, S. Shateyi, M.M. Rashidi, E. Momoniat, N. Freidoonimehr, MHD stagnation point flow heat and mass transfer of nanofluids in porous medium with radiation, viscous dissipation and chemical reaction, Adv. Powder Technol. 27 (2016) 742−749.

[27] J.C. Misra, S.D. Adhikary, MHD oscillatory channel flow, heat and mass transfer in a physiological fluid in presence of chemical reaction, Alexandria Eng. J. 55 (2016) 287−297.

[28] M.A.A. Mahmoud, S.E. Waheed, MHD flow and heat transfer of a micropolar fluid over a stretching surface with heat generation (absorption) and slip velocity, J. Egyptian Math. Soc. 20 (2012) 20−27.

[29] K. Das, Slip effects on MHD mixed convection stagnation point flow of a micro-polar fluid towards a shrinking vertical sheet, Comput. Math. Appl. 63 (2012) 255−267.

[30] N.C. Roşca, I. Pop, Boundary layer flow past a permeable shrinking sheet in a micropolar fluid with a second order slip flow model, European J. Mech. B/Fluids 48 (2014) 115−122.

[31] K. Das, S. Jana, P.K. Kundu, Thermophoretic MHD slip flow over a permeable surface with variable fluid properties, Alexandria Eng. J. 54 (2015) 35−44.

[32] P. Singh, A.K. Pandey, M. Kumar, Forced convection in MHD slip flow of alumina-water nanofluid over a flat plate, J. Enhanc. Heat Transf. 23 (6) (2016) 487−497.

[33] A.K. Pandey, M. Kumar, Natural convection and thermal radiation influence on nanofluid flow over a stretching cylinder in a porous medium with viscous dissipation, Alexandria Eng. J. 56 (1) (2017) 55−62.

[34] K. Singh, A.K. Pandey, M. Kumar, Analytical approach to stagnation-point flow and heat transfer of a micropolar fluid via a permeable shrinking sheet with slip and convective boundary conditions, Heat Tran. Res. 50 (8) (2019) 739−756.

[35] A. Mishra, A.K. Pandey, M. Kumar, Velocity, thermal and concentration slip effects on MHD silver-water nanofluid past a permeable cone with suction/injection and viscous-Ohmic dissipation, Heat Tran. Res. 50 (14) (2019) 1351−1367.

[36] R.A. Damseh, M.Q. Al-Odata, A.J. Chamkha, B.A. Shannak, Combined effect of heat generation or absorption and first-order chemical

reaction on micropolar fluid flows over a uniformly stretched permeable surface, Int. J. Therm. Sci. 48 (2009) 1658−1663.

[37] M.M. Rahman, A. Aziz, M.A. Al-Lawatia, Heat transfer in micropolar fluid along an inclined permeable plate with variable fluid properties, Int. J. Therm. Sci. 49 (2010) 993−1002.

[38] H. Rosali, A. Ishak, I. Pop, Micropolar fluid flow towards a stretching/shrinking sheet in a porous medium with suction, Int. Commun. Heat Mass Tran. 39 (2012) 826−829.

[39] S.Z.A. Zaidi, S.T. Mohyud-Din, Analysis of wall jet flow for Soret, Dufour and chemical reaction effects in the presence of MHD with uniform suction/injection, Appl. Therm. Eng. 103 (2016) 971−979.

[40] M. Sheikholeslami, D.D. Ganji, M.M. Rashidi, Magnetic field effect on unsteady nanofluid flow and heat transfer using Buongiorno model, J. Magn. Magn Mater. 416 (2016) 164−173.